Geophysical Journal International

Geophys. J. Int. (2010) **182,** 168–182 doi: 10.1111/j.1365-246X.2010.04634.x

Three-dimensional inversion of ZTEM data

Elliot Holtham and Douglas W. Oldenburg

UBC-Geophysical Inversion Facility, Department of Earth and Ocean Sciences, University of British Columbia, Vancouver, BC V6T 1Z4*, Canada.*
E-mail: eholtham@eos.ubc.ca

Accepted 2010 April 17. Received 2010 April 7; in original form 2009 June 1

SUMMARY

Z-Axis Tipper Electromagnetic Technique (ZTEM) data are airborne electromagnetic data which record the vertical magnetic field that results from natural sources. The data are transfer functions that relate the local vertical field to orthogonal horizontal fields measured at a reference station on the ground. The transfer functions depend on frequency and provide information about the 3-D conductivity structure of the Earth. The practical frequency range is 30–720 Hz and hence it is possible to see structures at depths of a kilometre or more if the earth is of moderate conductivity. This depth of penetration is significantly greater than that obtained with controlled source EM techniques and, when coupled with rapid spatial acquisition with an airborne system, means that ZTEM data can be used to map large-scale structures that are difficult to survey with ground based surveys. We present some fundamentals about understanding the signatures obtained with ZTEM transfer functions and then develop a Gauss–Newton algorithm to invert ZTEM data. The algorithm is applied to synthetic examples and to a field data set from the Bingham Canyon region in Utah. The field data set requires a workflow procedure to estimate appropriate noise levels in individual frequency components. These noise levels can then be used to invert multiple frequencies simultaneously. ZTEM data are insensitive to a 1-D conductivity structures and hence the background can be difficult to estimate. We provide two methods to determine appropriate background models. Interestingly, topography, which is usually a hinderance in field data interpretation, provides a first-order signal in the ZTEM data and helps with this calibration.

Key words: Inverse theory; Electromagnetic theory; Magnetotelluric.

1 INTRODUCTION

Natural source electromagnetics have an important role in understanding the electrical conductivity of upper regions of the earth. Their primary advantage, compared to controlled source methods, is the large depth of penetration that is a consequence of the plane wave excitation. The magnetotelluric (MT) method, uses ratios of electric and magnetic fields as data and it has played a significant role in crustal studies as well as in mining and hydrocarbon exploration. Its recognized importance, combined with increased computational abilities, has been the impetus for significant work in 3-D MT inversion (among others Mackie & Madden 1993; Newman & Alumbaugh 2000; Zhdanov *et al.* 2000; Farquharson *et al.* 2002; Sasaki 2004; Siripunvaraporn *et al.* 2005). A practical limitation of the MT technique and other deep probing controlled source electromagnetic methods, is that surveys are costly and time consuming because they are extremely labour intensive. It would be preferable to collect MT data in an aircraft but this goal has not yet been achieved because of the difficulty in measuring the electric fields.

In an effort to continue to use the penetration advantage of natural sources, it has long been recognized that tipper data, the ratio of the local vertical magnetic field to the horizontal magnetic field, provide information about 3-D electrical conductivity structure. The underlying reason is that the inducing electromagnetic fields are vertically propagating plane waves and if the earth is 1-D then the vertical component of the magnetic field is zero. Non-zero values of the tipper data are thus directly related to anomalous currents. It was this understanding that prompted the development of Audio Frequency Magnetics (AFMAG) technique (Ward 1959). The original airborne AFMAG technique used the amplitude outputs from two orthogonal coils towed behind an aircraft to determine the tilt of the plane of polarization of the natural magnetic field. The tilt angle is zero over a 1-D Earth and hence the technique was particularly effective when crossing conductors. However, because the direction and strength of the inducing field varied with time, AFMAG results were not always repeatable. Limitations of the AFMAG technique were outlined in Ward *et al.* (1966).

Some of the AFMAG problems can be removed by using improved signal processing and data acquisition techniques. In particular, Labson *et al.* (1985) developed a technique that used ground based horizontal and vertical coils to measure the magnetic fields. They used MT processing techniques to show how tipper data could be obtained from the measured magnetic fields.

A further improvement to the original AFMAG technique combines improved instrumentation and MT data processing techniques. This has resulted in the *Z*-Axis Tipper Electromagnetic Technique (ZTEM) (Lo & Zang 2008). In ZTEM, the vertical component of the magnetic field is recorded above the entire survey area, while the horizontal fields are recorded at a ground-based reference station. MT processing techniques yield frequency domain transfer functions that relate the vertical fields over the survey area to the horizontal fields at the reference station. By taking ratios of the two fields (similar to taking ratios of the E and H fields in MT), the effect of the unknown source function is removed. Since new instrumentation exists to measure the vertical magnetic fields by helicopter, data over large survey areas can quickly be collected. The result is a cost effective procedure for collecting natural source EM data that provide information about the 3-D conductivity structure of the earth. Over the last several years industry has recognized the potential in this technique and the need to be able to invert these data.

In this paper, we present a 3-D inversion algorithm for ZTEM data. Forward modelling is fundamental to any inversion algorithm and we first show how to model the magnetic transfer functions. A simple example is used to illustrate the principles associated with ZTEM data. Next, we present our algorithm for inverting ZTEM data and apply it to a synthetic test problem. Finally, the technique is tested on a field data set from the Bingham Canyon region in Utah. We discuss practical issues of implementing the inversion and develop a workflow methodology to make the procedure more efficient.

1.1 ZTEM system and data acquisition

ZTEM instrumentation, developed by Geotech Inc, uses a helicopter to tow a coil which measures the vertical component of the magnetic field. Orthogonal coils from a single reference station measure the horizontal components of the magnetic field. The essential components of the system can be seen in Fig. 1. Time-series of the magnetic fields are recorded with a fixed sampling rate and data are binned and processed to generate transfer functions in the frequency domain. The lowest frequency of the transfer function depends upon the speed of the helicopter, and the highest depends upon the sampling rate, signal strength and noise. Although frequencies up to 2800 Hz are potentially available, in practise the useable bandwidth is about 22–720 Hz. The lower frequency has a skin depth of 3300 m in a 1000 Ωm background and 330 m for a 10 Ωm background. These are depth limits that are extremely difficult to achieve with controlled source ground or airborne systems.

1.2 Magnetic transfer functions

ZTEM data are transfer functions that relate the vertical magnetic fields computed above the earth to the horizontal magnetic field at some fixed reference station. This relation is given by

$$H_z(r) = T_{zx}(r, r_0)H_x(r_0) + T_{zy}(r, r_0)H_y(r_0), \tag{1}$$

where r is the location for the vertical field, r_0 is the location of the ground based reference station and T_{zx} and T_{zy} are the vertical field transfer functions. Solving for the transfer functions requires that the vertical fields are known for two independent polarizations. The fields for each polarization are given by

$$H_z^{(1)} = T_{zx}H_x^{(1)} + T_{zy}H_y^{(1)}, \tag{2a}$$

$$H_z^{(2)} = T_{zx}H_x^{(2)} + T_{zy}H_y^{(2)}, \tag{2b}$$

or

$$\begin{pmatrix} H_z^{(1)}(r) \\ H_z^{(2)}(r) \end{pmatrix} = \begin{pmatrix} H_x^{(1)}(r_0) & H_y^{(1)}(r_0) \\ H_x^{(2)}(r_0) & H_y^{(2)}(r_0) \end{pmatrix} \begin{pmatrix} T_{zx} \\ T_{zy} \end{pmatrix}, \tag{3}$$

where the superscripts (1) and (2) refer to the source field polarization in the x and y directions, respectively. Solving eq. (3) yields the following expressions for the transfer functions,

$$T_{zx} = \frac{H_y^{(2)}H_z^{(1)} - H_y^{(1)}H_z^{(2)}}{H_x^{(1)}H_y^{(2)} - H_x^{(2)}H_y^{(1)}}, \tag{4a}$$

$$T_{zy} = \frac{-H_x^{(2)}H_z^{(1)} + H_x^{(1)}H_z^{(2)}}{H_x^{(1)}H_y^{(2)} - H_x^{(2)}H_y^{(1)}}. \tag{4b}$$

To forward model the transfer functions, one must have the capability to solve the natural source field problem for different polarizations of the source field. A procedure to do this is presented next.

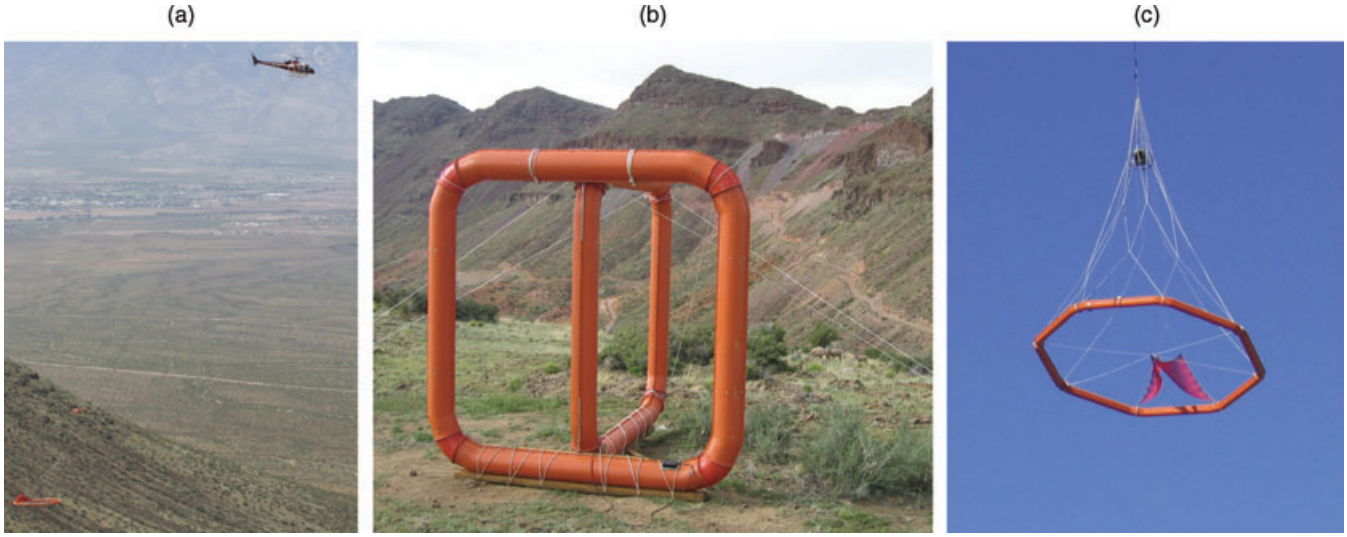

Figure 1. (a) Helicopter flying a coil to measure the vertical magnetic field. (b) Ground based reference station. (c) Coil used to measure the vertical fields.

1.3 Forward modelling

Our forward modelling procedure is essentially that outlined in Farquharson *et al.* (2002), where the solution of Maxwell's equations is that of Haber *et al.* (2000). In brief, Maxwell's equations in the quasi-static regime, when combined with the constitutive relations of charge conservation and Ohm's law, form the necessary equations for ZTEM modelling. These equations read,

$$\nabla \times \mathbf{E} - \mathrm{i}\omega\mu\mathbf{H} = 0, \tag{5a}$$

$$\nabla \times \mathbf{H} - \sigma\mathbf{E} = 0, \tag{5b}$$

$$\nabla \cdot \mathbf{J} = 0, \tag{5c}$$

$$\mathbf{J} - \sigma\mathbf{E} = 0, \tag{5d}$$

where $\mathbf{E}$ is the electric field, $\mathbf{H}$ is the magnetic field, ω is the angular frequency, σ is the conductivity, and $\mathbf{J}$ is the current density. We have assumed an $\mathrm{e}^{-\mathrm{i}\omega t}$ time-dependence and that the magnetic permeability μ is constant and equal to that of free space, μ_0. To solve for the fields, the electric field is decomposed into vector and scalar potentials $\mathbf{E} = \mathbf{A} + \nabla\phi$ and the Coulomb gauge condition $\nabla \cdot \mathbf{A} = 0$ is imposed for uniqueness. Using the decomposition and eliminating $\mathbf{H}$ yields the potential equations

$$\nabla^2\mathbf{A} + \mathrm{i}\omega\mu_0\sigma(\mathbf{A} + \nabla\phi) = 0, \tag{6}$$

$$\nabla \cdot \mathbf{J} = \nabla \cdot [\sigma(\mathbf{A} + \nabla\phi)] = 0. \tag{7}$$

For our modelling we discretize the earth into rectangular cells and, after applying a finite volume technique (Haber *et al.* 2000) to eqs (6) and (7), we obtain the system of equations to be solved. In this staggered discretization, the scalar potential is defined on the cell centres while the vector potential is defined by the normal components at the centre of the cell faces. To solve for the total fields we use a primary-secondary decomposition. The primary fields equations, which must only be solved once on the background conductivity model, are

$$\begin{pmatrix} \mathbf{L} + \mathrm{i}\omega\mu_0\mathbf{S} & \mathrm{i}\omega\mu_0\mathbf{SG} \\ \mathbf{DS} & \mathbf{DSG} \end{pmatrix} \begin{pmatrix} \mathbf{A_p} \\ \phi_p \end{pmatrix} = 0. \tag{8}$$

$\mathbf{A}_\mathrm{p}$ are the primary vector potentials on the mesh and ϕ_p are the primary scalar potentials. $\mathbf{L}$ represents the discretization of the Laplacian operator, $\mathbf{S}$ represents the harmonically averaged background cell conductivities, and $\mathbf{G}$ and $\mathbf{D}$ are the discretizations of the gradient and divergence operators. The normal component of $\mathbf{J}$ and the tangential component of $\nabla \times \mathbf{A}$ are specified on the boundary by computing the appropriate one and 2-D boundary values. Once the background fields have been calculated, the source term is known for the secondary field calculation. The equations for the secondary field are

$$\begin{pmatrix} \mathbf{L} + \mathrm{i}\omega\mu_0\mathbf{S} & \mathrm{i}\omega\mu_0\mathbf{SG} \\ \mathbf{DS} & \mathbf{DSG} \end{pmatrix} \begin{pmatrix} \mathbf{A_s} \\ \phi_s \end{pmatrix} = \begin{pmatrix} -\mathrm{i}w\mu_0\Delta\mathbf{SE_p} \\ -\mathbf{D}\Delta\mathbf{SE_p} \end{pmatrix}, \tag{9}$$

where $\Delta\mathbf{S} = \mathbf{S} - \mathbf{S}_\mathrm{p}$ is the difference between the averaged conductivities of the actual model and those of the background, and $\mathbf{E}_\mathrm{p}$ is the primary electric field. For the secondary formulation the secondary potentials are assumed to vanish on the mesh boundaries. For each source polarization (one for an x-directed H-field at the top of the mesh, and the other for a y-directed H-field) the resulting H fields are computed.

1.4 Currents and transfer functions

Since a 1-D earth produces no vertical magnetic fields, it is deviations from a 1-D conductivity structure that causes a ZTEM response. With the addition of two and 3-D structure, new anomalous currents will flow in the earth. It is these anomalous currents,

$$\mathbf{J_{anomalous}} = \mathbf{J_{total}} - \mathbf{J_{primary}} \tag{10}$$

the give rise to vertical magnetic fields. We investigate the currents and associated vertical magnetic fields by considering the models in Fig. 2 of conductive and resistive prisms in a moderate conductivity host. Fig. 3 shows the anomalous current density, computed using the 3-D forward modelling code described in the previous section, for a vertical slice through the prisms. The anomalous current is fairly uniform and strongest inside the block. The magnetic field and transfer functions (Fig. 4) look like that obtained from an extended dipole current. The anomalous currents for a resistive block flow in the opposite direction compared to the conductive block. For Fig. 4, the T_{zx} transfer functions correspond to the electric field

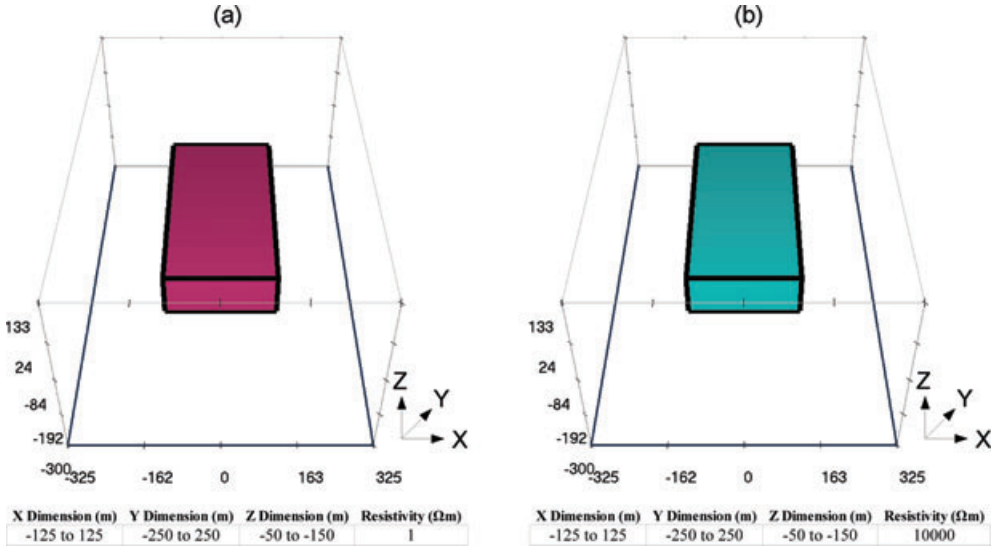

Figure 2. (a) 1 Ωm conducting block buried in a 200 Ωm background. (b) 10 000 Ωm resistive block buried in a 200 Ωm background.

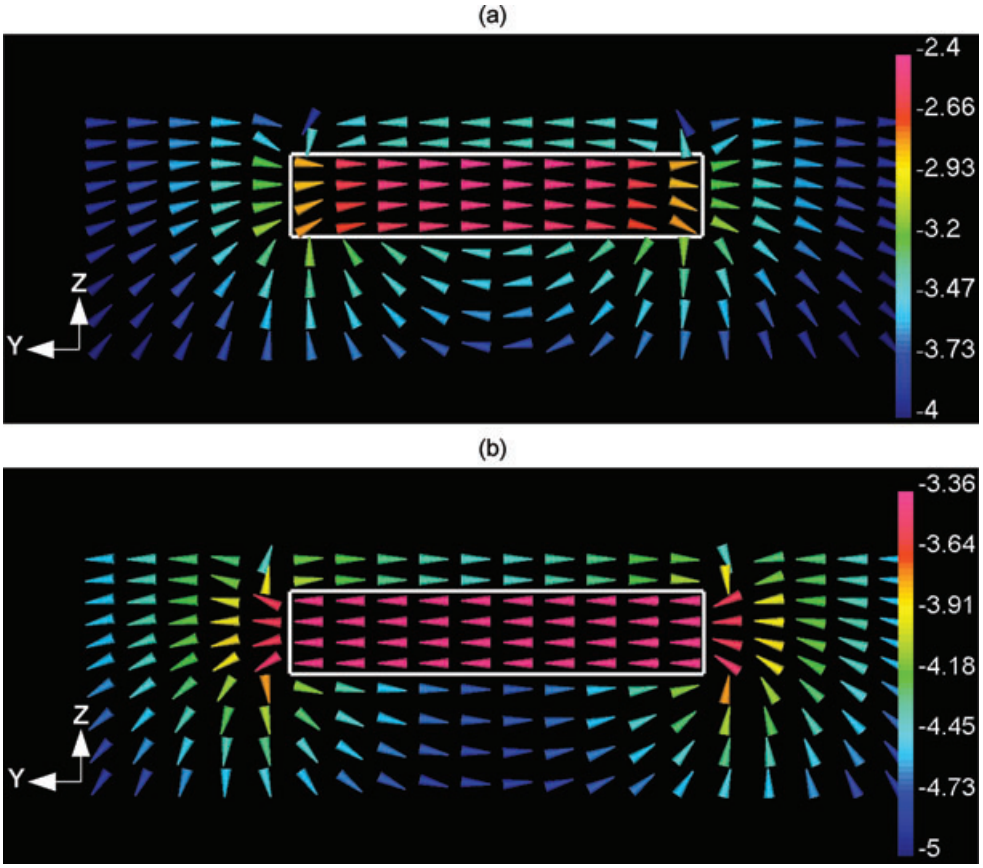

Figure 3. The real anomalous current densities $[\mathrm{Log}_{10}(\frac{A}{m^2})]$ in the z–y plane ($x = -25$ m) for a source whose electric field is polarized in the $(-\hat{y})$ direction. The white rectangles are the outlines of the original blocks. Panel (a) is the current for the conductive block, while panel (b) is the current for the resistive block. The anomalous current is mostly localized inside the block.

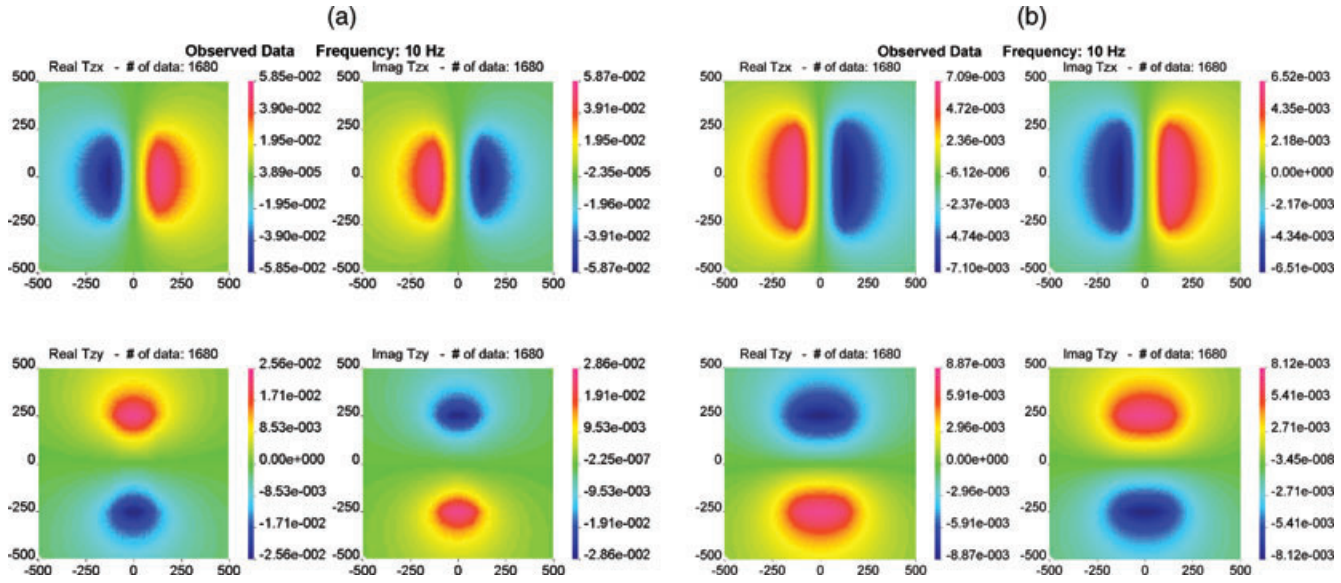

Figure 4. Resulting transfer functions for the two block example of Fig. 2. Panel (a) corresponds to a conductive block while panel (b) corresponds to a resistive block. The transfer functions closely resemble the magnetic fields due to a finite line current inside the blocks.

polarized in $-\hat{y}$, while the T_{zy} response corresponds to the orthogonal polarization where the electric field is in $\hat{x}$. The direction of the anomalous current determines the sign of the response while the distance between positive and negative maxima is related to the size of the block.

2 INVERSE PROBLEM

For simple geometries the concepts of anomalous currents can help interpret ZTEM data. For instance, a linear filter can be applied to the vertical magnetic field (Karous & Hjelt 1983) to generate current

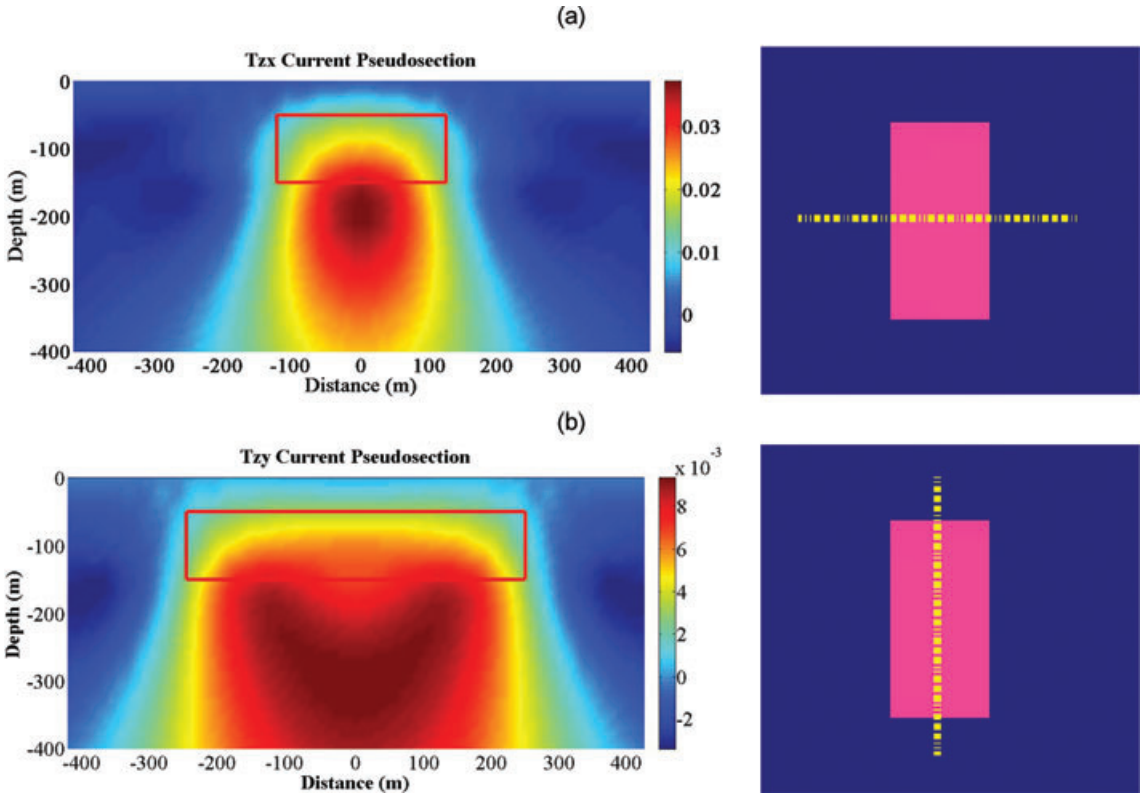

Figure 5. Current pseudo-section obtained by linear filtering the transfer functions for the model in Fig. 2. Panel (a) is the linear filtering of the T_{zx} transfer function along the cross section $y = 0$ m. Panel (b) is the filtering of the transfer function T_{zy} along the cross section $x = 0$ m. The true outline of the conducting block is superimposed in red. For this simple example, linear filtering the two transfer functions gives an indication about the lateral boundaries of the block.

pseudo-sections. An example of filtering the real components of the transfer functions produced from the conductive model in Fig. 2 is shown in Fig. 5. These plots were generated using the Matlab code of Sundararajan et al. 2006. For this simple block in a half-space example, the block geometry may be adequately interpreted from the current pseudo-sections. Nonetheless, in the case of complex 3-D models, 3-D inversions are necessary.

Our inversion algorithm is based on the MT inversion code of Farquharson *et al.* (2002). By minimizing the objective function

$$\Phi = \phi_d + \beta\phi_m, \tag{11}$$

we obtain our solution to the inverse problem. ϕ_d is the data-misfit, ϕ_m is amount of structure in the model and β is the trade-off or regularization parameter. We use the sum of squares as the measure of misfit

$$\phi_d = \left\| \mathbf{W_d}(\mathbf{d^{obs}} - \mathbf{d^{prd}}) \right\|_2^2, \tag{12}$$

where $\mathbf{d}^{\text{obs}}$ is the observation vector, $\mathbf{d}^{\text{prd}}$ is the vector of predicted data and $\mathbf{W}_d$ is a diagonal matrix whose elements are the reciprocals of the standard deviations of the data errors. The measure of model

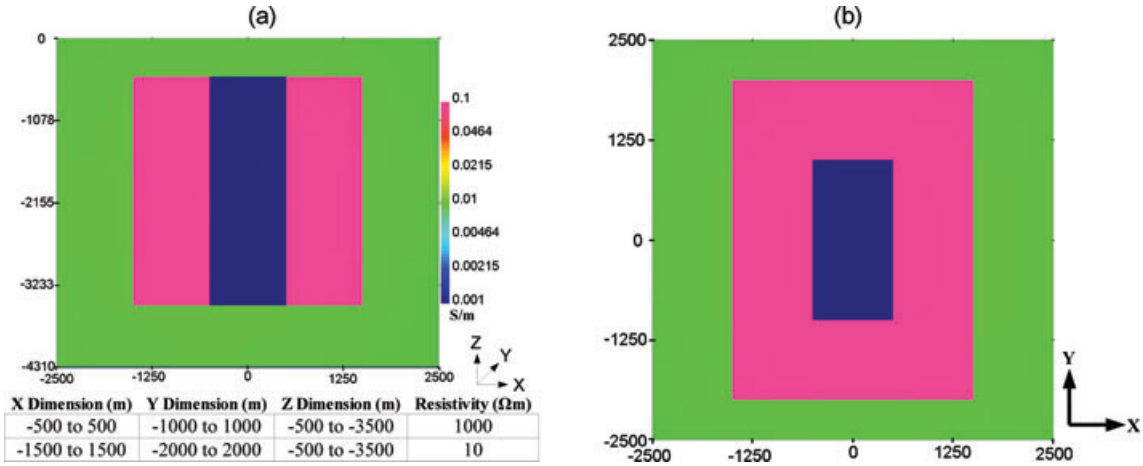

X Dimension (m)	Y Dimension (m)	Z Dimension (m)	Resistivity (Ωm)
-500 to 500	-1000 to 1000	-500 to -3500	1000
-1500 to 1500	-2000 to 2000	-500 to -3500	10

Figure 6. Conductivity model: a resistor surrounded by a conductor, all buried in a 100 Ωm background half-space. (a) Cross-section through $y = 0$ m. The bottom table summarizes the block dimensions and resistivities. (b) Depth slice at 1000 m.

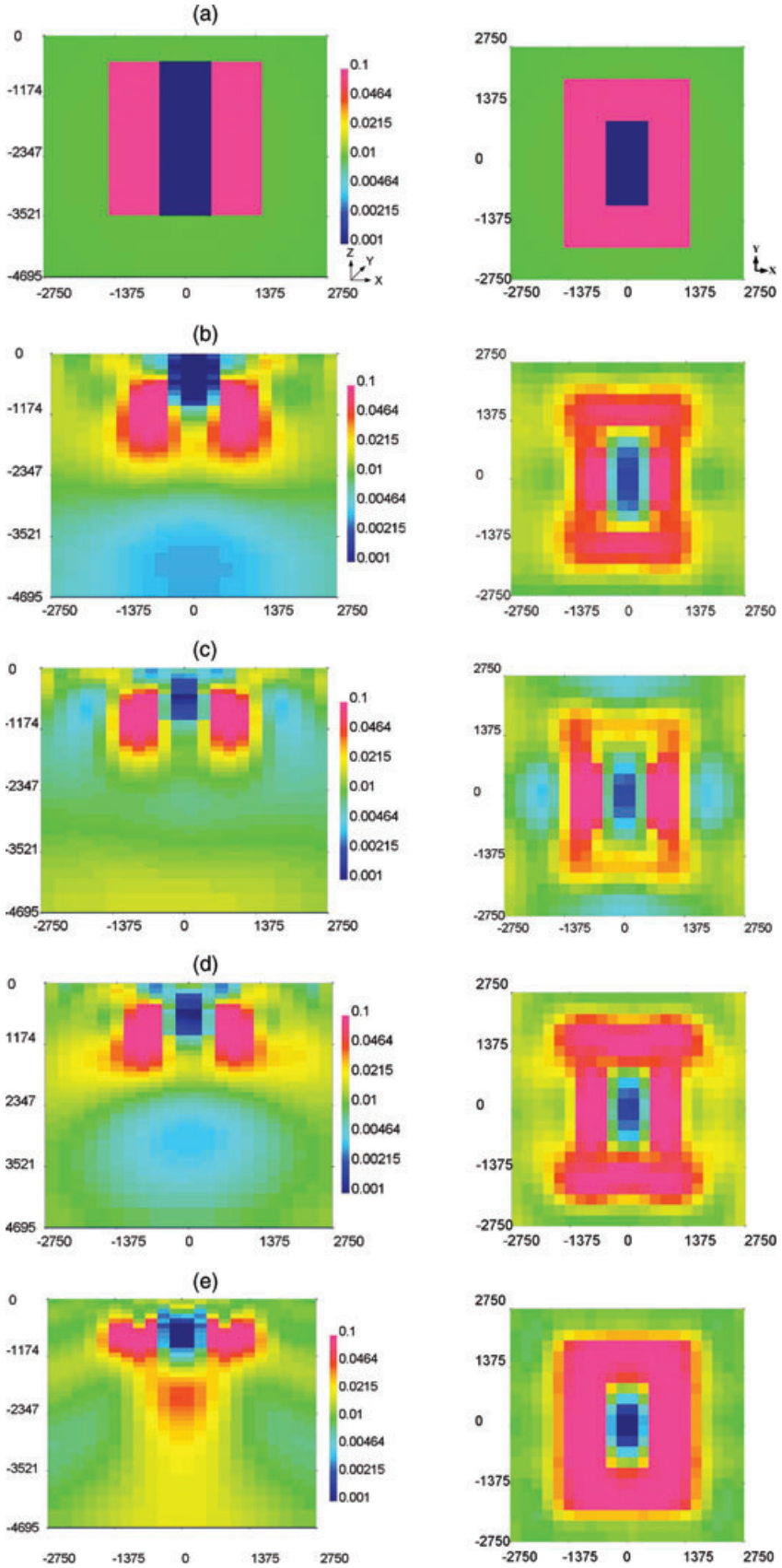

Figure 7. Conductivity model ($S\,m^{-1}$) from the inversion of the synthetic model data. Figure (a) is a cross section at the centre of the model and a plan view section at a depth of 800 m. Panels (b)–(d) are results of inverting data at 1 Hz. Panel (b) is the inversion of the real parts, panel (c) is the imaginary parts and panel (d) is the real and imaginary components. Panel (e) is the simultaneous inversion of six frequencies.

structure is

$$\phi_m = \alpha_s \left\| \mathbf{W}_s(\mathbf{m} - \mathbf{m}^{\text{ref}}) \right\|_2^2 + \alpha_x \left\| \mathbf{W}_x(\mathbf{m} - \mathbf{m}^{\text{ref}}) \right\|_2^2 + \alpha_y \left\| \mathbf{W}_y(\mathbf{m} - \mathbf{m}^{\text{ref}}) \right\|_2^2 + \alpha_z \left\| \mathbf{W}_z(\mathbf{m} - \mathbf{m}^{\text{ref}}) \right\|_2^2,$$

where $\mathbf{W}_s$ is a diagonal matrix and $\mathbf{W}_x$, $\mathbf{W}_y$ and $\mathbf{W}_z$ are the first-order finite-difference matrices in the x, y and z directions, and $\mathbf{m}^{\text{ref}}$ is a reference model. The $\alpha's$ are adjustable parameters. α_s controls the closeness of the recovered model to the reference, while $\alpha_{x,y,z}$ determine the smoothing in the x, y and z directions. For the minimization of the objective function at the $(n+1)$th iteration, the Gauss–Newton method requires the solution of

$$\left(\mathbf{J}^T\mathbf{W}_d^T\mathbf{W}_d\mathbf{J} + \beta\mathbf{W}^T\mathbf{W}\right)\delta\mathbf{m} = -\mathbf{J}^T\mathbf{W}_d^T\mathbf{W}_d(\mathbf{d}^{\text{obs}} - \mathbf{d}^n) - \beta\mathbf{W}^T\mathbf{W}(\mathbf{m}^n - \mathbf{m}^{\text{ref}}), \quad (13)$$

where $\mathbf{m}^n$ is the vector of model parameters from the previous iteration, $\mathbf{J}$ is the Jacobian matrix of sensitivities, $\mathbf{W}$ is such that $\mathbf{W}^T\mathbf{W} = \sum \alpha_k \mathbf{W}_k^T\mathbf{W}_k$, and $\delta\mathbf{m}$ is the model perturbation. Since ZTEM data are different than MT data, the Jacobian matrix must be modified accordingly. The implementation however follows that outlined in Farquharson *et al.* (2002). Eq. (13) is solved using an inexact preconditioned conjugate gradient (IPCG) (Saad 2003) algorithm. Typically, 5 IPCG iterations are performed to solve equation (13) for each value of β. Since $\mathbf{J}$ is prohibitively large to compute, this solution method only requires the sparse matrix operations $\mathbf{W}^T\mathbf{W}$, $\mathbf{J}$, $\mathbf{J}^T$ on a vector. β is initially chosen to be large such that $\beta\mathbf{W}^T\mathbf{W}$ dominates the approximate Hessian in eq. (13). It is then reduced in a cooling schedule such that at each subsequent iteration $\beta_{k+1} = \gamma\beta_k$, where γ is a constant. Efficient implementation of this inversion in application to field data sets requires a workflow procedure but we postpone details about that until Section 4.

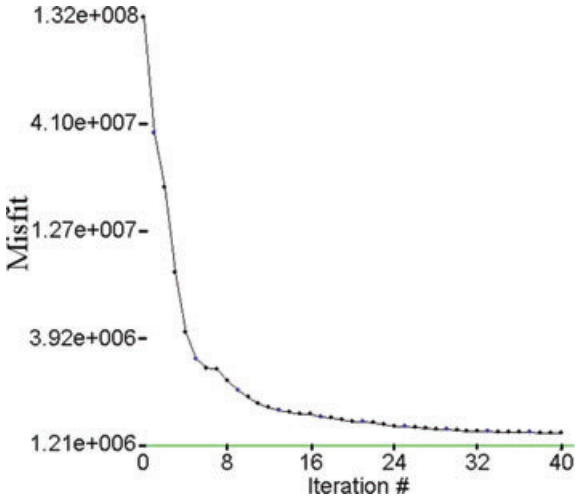

Figure 8. Convergence curve for the inversion of six frequencies for the synthetic inversion model. The algorithm reduced the misfit to 1.38×10^6 (target misfit 1.21×10^6)

3 SYNTHETIC INVERSION

We illustrate the inversion of ZTEM data using a synthetic example that was chosen to emulate a porphyry deposit. The model has a central resistive core, an outer region of high conductivity, and is buried in a moderate conductivity background. The conductivity structure is shown in Fig. 6. The Earth was discretized into a mesh containing $42 \times 42 \times 57$ cells in the x, y and z directions, respectively. The cell dimensions in the central core region were $250 \times 250 \times 100$ m in the x, y and z directions, respectively. The vertical fields at 1, 3.2, 5.6, 10, 18 and 32 Hz were computed at a fixed height of 100 m over the surface. This frequency range is shifted somewhat from the traditional ZTEM survey but this is inconsequential for the purpose of testing the code. The data were computed at 10 m intervals and 50 m line-spacing over a 5 km $\times$ 5 km region. The horizontal field components were computed at a ground based reference station at a location r_0 of $x = -3000$ m, $y = -3000$ m. For each component of each frequency Gaussian noise, equal to 3.5 per cent of the difference between the 10th percentile and 90th percentile data, was added. The initial model and reference models were homogeneous half-spaces of 100 Ωm. We first inverted different subsets of the data to determine their information content. The 1 Hz data were inverted with the real and imaginary components separately and then the 1Hz data were inverted with both the real and imaginary components. From the two sections of the model

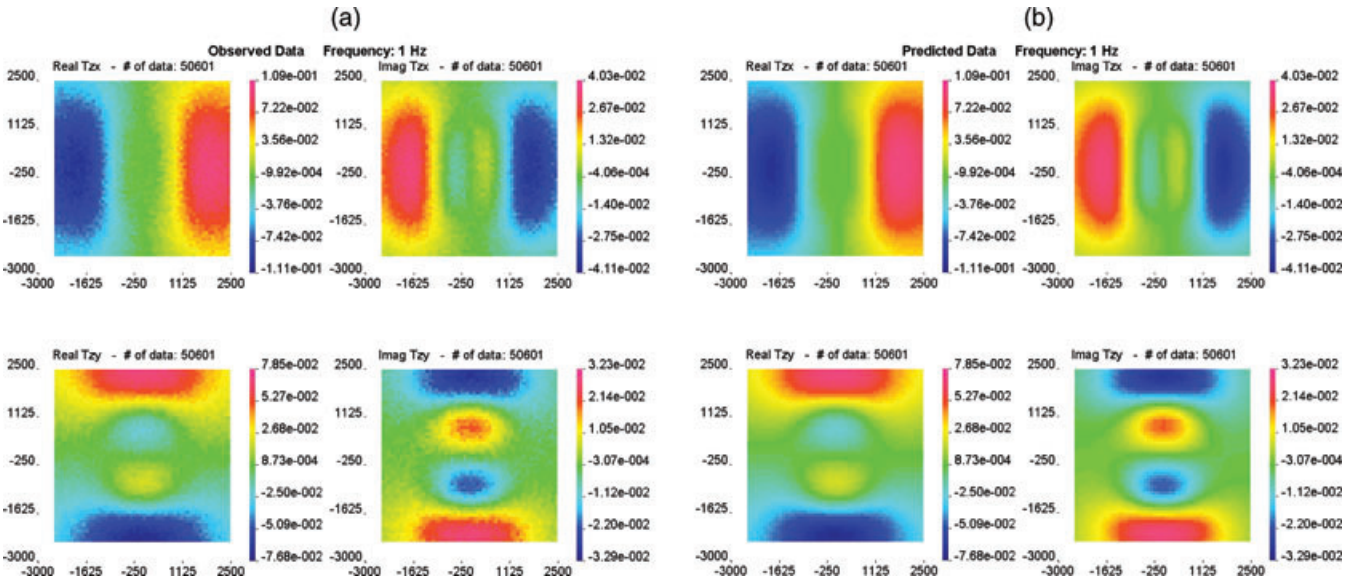

Figure 9. Panel (a) is the observed data and panel (b) is the predicted data for the synthetic model at 1 Hz. There is excellent agreement between the observed and predicted data.

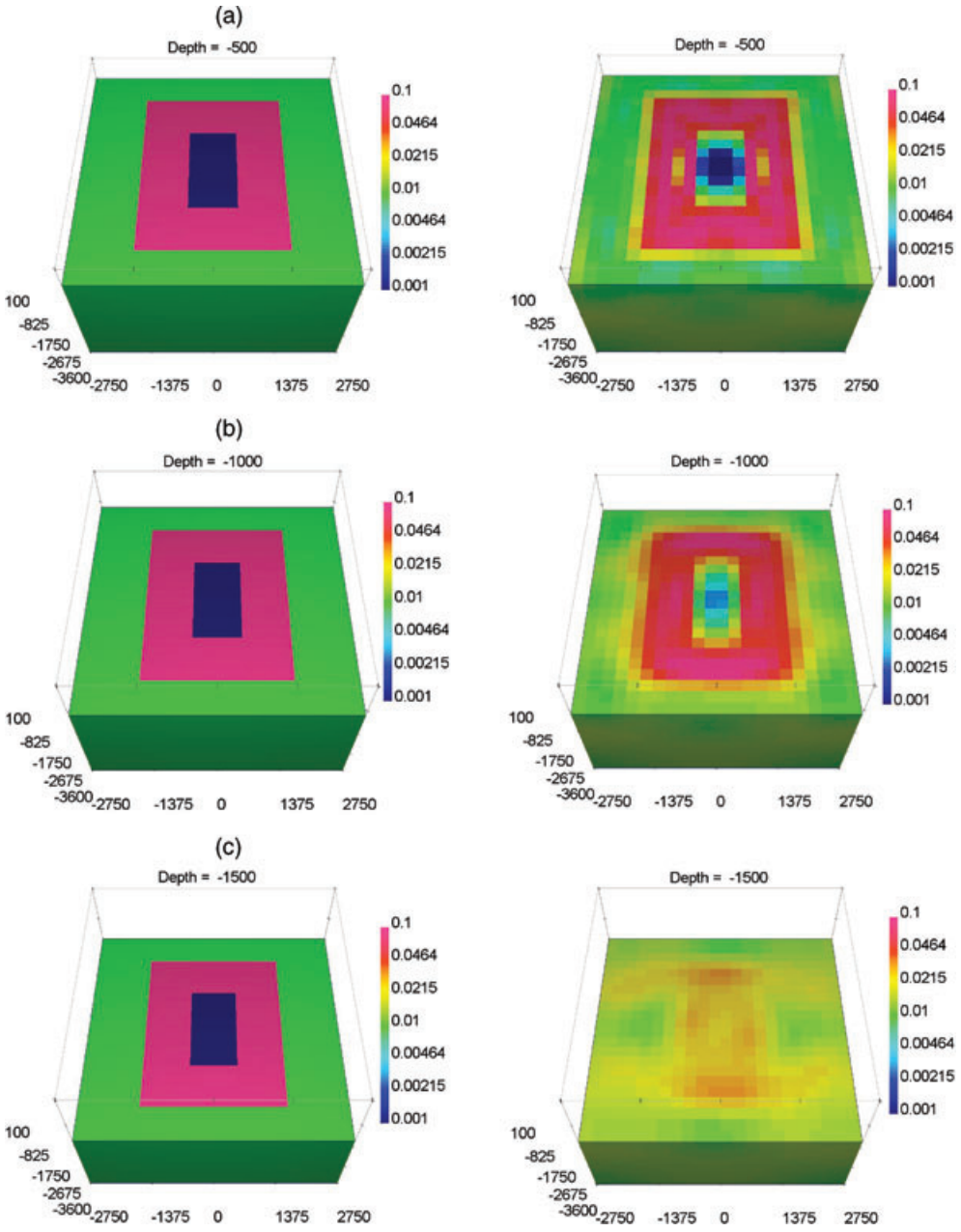

Figure 10. Conductivity model ($S\,m^{-1}$) from the inversion of the synthetic model using six frequencies. Slices of the true model (left-hand panels) and recovered model (right-hand panels) are shown at 500, 1000 and 1500 m.

inversions in Fig. 7, it is clear that both the real and imaginary components contain significant information and that both components of the data should be obtained in a ZTEM survey. Since 1 Hz is the lowest frequency used, it also resolves the deepest structure. Next all six frequencies were inverted simultaneously. The inversion was executed in parallel over 6 dual processors. The convergence curve for the inversion is shown in Fig. 8. The recovered model fits the data well and select data are shown in Fig. 9. The final model in Fig. 10 recovers both the conductivity and block dimensions in the x and y directions very well. There is significant improvement in the block resolution in the x and y directions over the single 1 Hz inversion. The inverted result shows that the top interface is well resolved, however, the base of the blocks are not. This is consistent with skin depth arguments of the lowest frequency.

3.1 Effect of the reference station

An important component of the ZTEM survey is the reference station that is used to compensate for the unknown source amplitude and polarization. The transfer functions are the ratio of the vertical fields to the horizontal field at the reference station. Ideally the fields at the reference station are those due to a 1-D conductivity structure; however this is not necessary for two reasons. First, the variation between the horizontal fields at the reference station and the observation point are generally small even if there are lateral changes in conductivity. Second, the location of the reference station is included in the modelling, and no assumptions have been made about the conductivity structure between the reference station and the observation point. To illustrate that the choice of reference

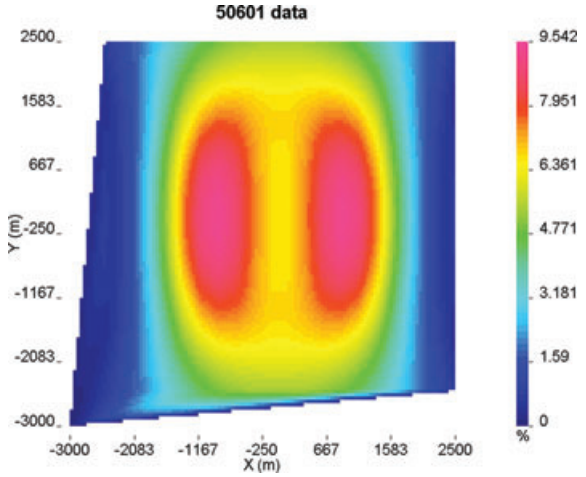

Figure 11. Per cent difference in the $\hat{x}$ component of the magnetic field between the reference location and the measurement location (source electric field in the $-\hat{y}$ direction).

station does not drastically change the inversion result, we compute the relative difference, $\frac{||(H_x(r)-H_x(r_{ref})||}{||H_x(r_{ref})||}$ for one source polarization on the synthetic inversion model using a reference station at $x = -3000$ m, $y = -3000$ m. As can be seen in Fig. 11 the variations in the horizontal fields are less than 9.5 per cent over the entire survey area.

The location of the maximum deviations of 9.5 per cent occurs at $x = -900$ m, $y = 0$ m. We now recompute the data using a new reference station located at this point of maximum deviation. We invert the new data keeping all other aspects of the inversion unchanged from the inversion using a reference station at $x = -3000$ m, $y = -3000$ m. The comparison between the two inversion results can be seen in Fig. 12. As we would expect, when the reference location is correctly modelled, the inversion result is not strongly dependent upon the location of the reference station.

A more interesting example concerns the result of working with an incorrect location of the reference station. In some surveys, the model domain can be excessively large if the remote is far away from the survey area. It would be desirable to have an artificial location for the reference station inside the modelling domain. We simulate this by computing the data using the reference location outside the survey area ($x = -3000$ m, $y = -3000$ m), and then mislocating the reference location to $x = -900$ m, $y = 0$ m during the inversion. By misplacing the reference station, we are in essence scaling the data by a factor that depends on the difference in horizontal fields between the true location and the new reference location. The results from this inversion in Fig. 12 show that even if the reference station is misplaced to the worst location, we may still recover a reasonable model.

4 3-D INVERSION OF ZTEM FIELD DATA

In the winter of 2008, field data were acquired by Exploration Syndicate Inc. over a 15 km × 20 km area adjacent to the Bingham Canyon mine in Utah. The data were collected as time-series which were then stacked and processed into transfer functions using proprietary Geotech software. The results were filtered and attitude corrected. The terrain in the survey block is extremely rugged which makes it challenging to interpret the data. During the survey, 495.5 line kilometres of data (real and imaginary components) were acquired at five frequencies (30, 45, 90, 180 and 360 Hz). To complicate the problem, a significant portion of the data was affected by cultural noise and needed to be removed before the data could be inverted.

The 3-D inversion of any geophysical field data set is a complex and time consuming process that requires a logical work flow in order to be completed accurately and efficiently. We present our workflow in (Fig. 13). In this section of the paper, we invert the field data and at the same time illustrate some specific parts of this workflow.

4.1 Discretizing the earth

To solve the necessary differential equations, the Earth must be discretized into a mesh and the discrete system for Maxwell's equations formed. In this discretization step a compromise must be achieved between the numerical accuracy in the forward modelling and the computational resources required. As with MT discretization problems, the usual guidelines that cell sizes must not violate skin depth rules apply. Unique to the ZTEM problem is that the reference station may be located far from the region of interest. This may increase the number of cells in the model because it is necessary to keep the cells small in order to accurately model the fields at the reference station. Also, since ZTEM data are very sensitive to topography, it is important to finely discretize the topography. These requirements, when combined with the high frequency and large geographic areas covered in ZTEM surveys, can require large meshes and significant computational overhead.

Due to large survey areas and extremely rugged topography it was challenging to obtain an efficient discretization for the Bingham Canyon survey. The topography was obtained from the United States National Elevation Database (Fig. 14). The Earth was discretized into a mesh containing 96 × 92 × 95 cells in the x, y and z directions. Over a single flight path the elevation could change by over 3000 ft and over the entire model the elevation changed by 4000 ft. The central region had 78 × 65 × 54 cells that were 250 m × 250 m × 50 m in the x, y and z directions. This 50 m vertical cell dimension allowed for the topography to be reasonably modelled. To keep the number of cells in the mesh as small as possible, during the inversion the location of the reference station was moved closer to the ZTEM lines.

4.2 Determining a background model

In the MT problem, where electric fields are measured, the background can be chosen either using the apparent resistivities or by choosing the half-space conductivity which minimizes the data misfit between the half-space data and the true data. These methods cannot be used for ZTEM since all 1-D conductivity models produce zero data. Nevertheless, the anomalous currents and data are affected by the background conductivity for 3-D models. Our experience shows that it is important to initialize the inversion with a good estimate of the background conductivity, especially if the anomalous bodies are deeply buried. If this is not done, then the inversion may recover a reasonable estimate of the relative conductivities, but fail to adequately reproduce the data and also be a poor approximation to the true model. We illustrate these principals by starting the 1 Hz inversion of the synthetic model with an initial background of 10 000 Ωm instead of the 100 Ωm true background. The model smallness parameter, α_s, was set to be 0 so that the reference model does not affect the inversion. From the misfit curve in Fig. 15 we see that the inversion was initially able to significantly reduce the misfit. During the first part of the inversion, some

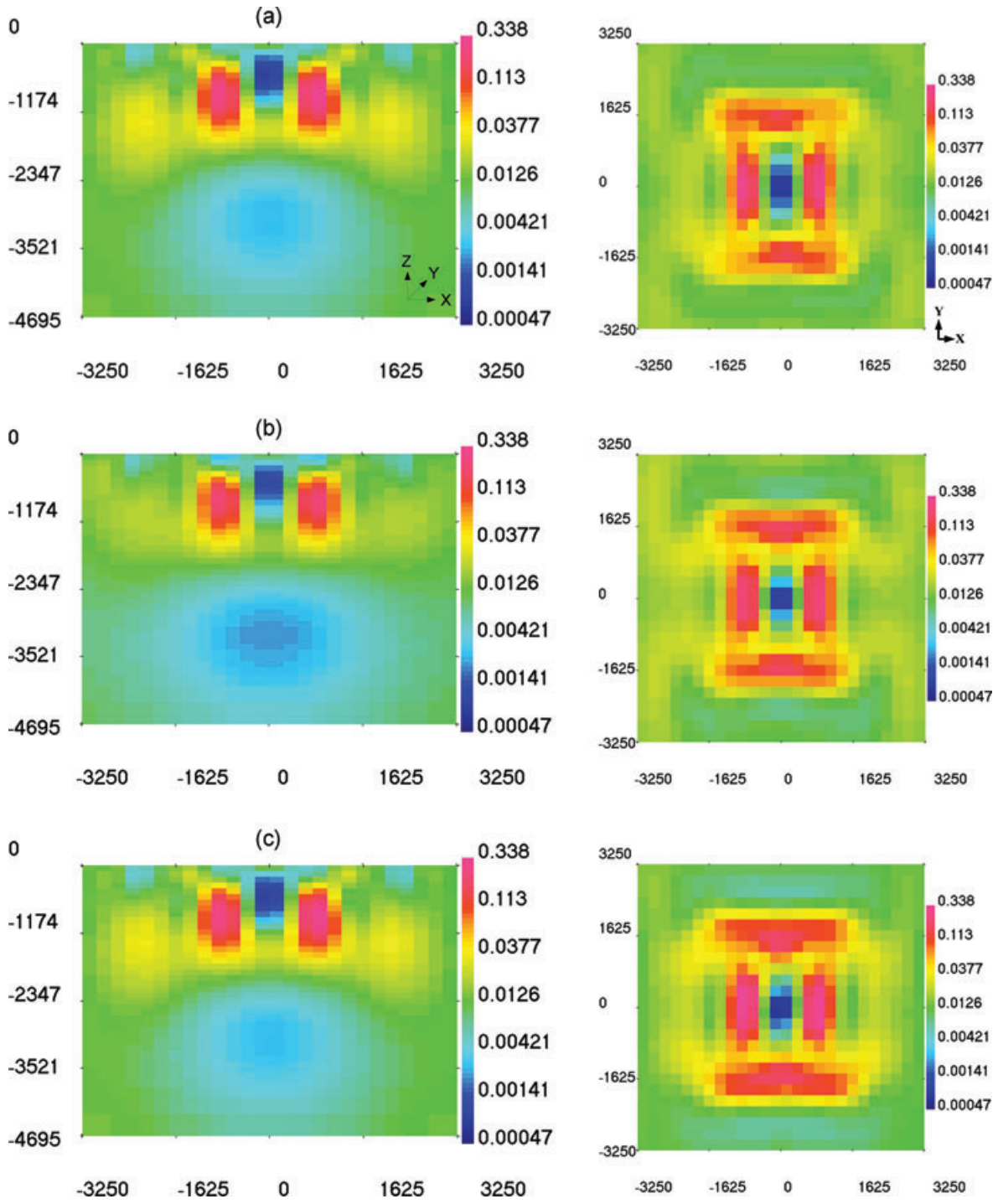

Figure 12. Conductivity model (S m^{-1}) from the inversion of the synthetic model data using different reference station locations. Figure (a) is a cross section at the centre of the model and a plan view section at a depth of 800 m that corresponds to a reference station located at $x = -900$ m, $y = 0$ m. For each inversion all of the parameters except the location of the reference station remain unchanged. Panel (a) corresponds to a reference station located at $x = -3000$ m, $y = -3000$ m. panel (b) corresponds to a reference station located at $x = -900$ m, $y = 0$ m. Panel (c) corresponds to data computed using a reference station at $x = -3000$ m, $y = -3000$ m, but during the inversion process the reference station is mislocated at $x = -900$ m, $y = 0$ m.

estimate of the relative conductivity has been established, however, it becomes increasingly difficult to fit the data since the background conductivity is drastically incorrect. Eventually, the inversion algorithm terminates with the final model in Fig. 15. Clearly, this is not a satisfactory result.

This inversion result motivated the following procedure. We used the inversion shown in Fig. 15 but selected a model just prior to the sharp change in slope on the misfit curve. We assumed that the relative conductivities on that model were correct. That conductivity was scaled by various constants and the data from the models were computed. The misfit between the true data and data produced from the scaled models is shown in Fig. 16. The smallest data misfit occurred when the conductivity of the preliminary model was scaled by a factor of 10. The conductivity in the survey area of the scaled

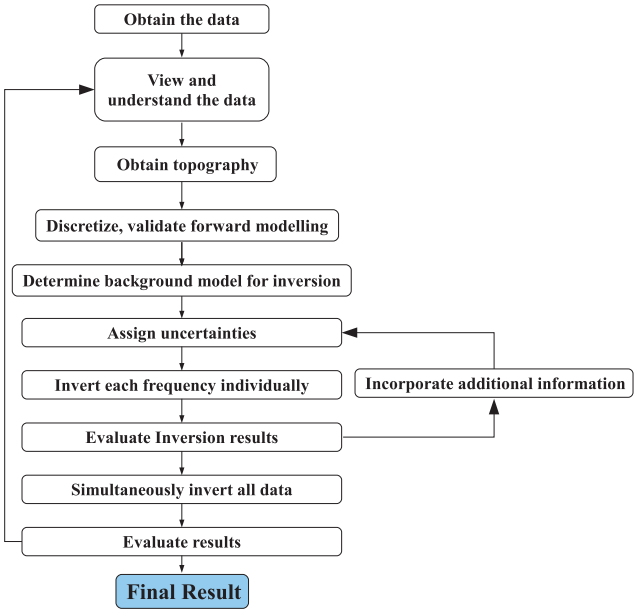

Figure 13. Work flow process summarizing the critical step in a ZTEM inversion.

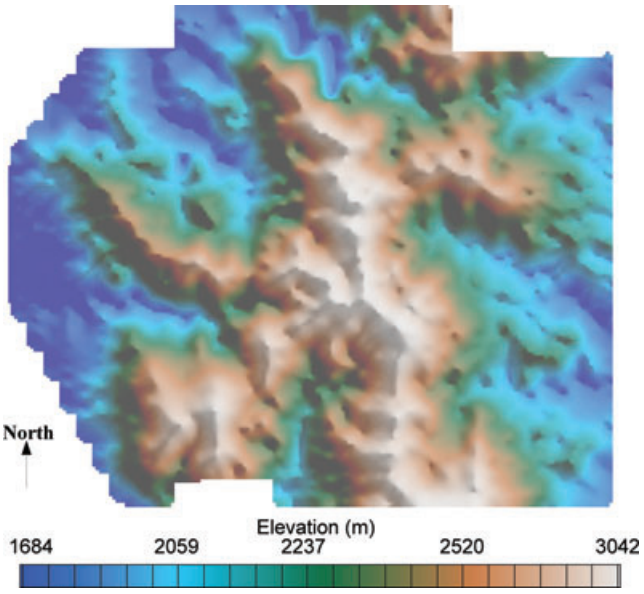

Figure 14. Topography from survey area near Bingham Canyon.

model was then averaged to obtain a background conductivity. This new conductivity was determined to be 169 Ωm instead of the actual 100 Ωm. This procedure of determining relative conductivities, scaling, and averaging, provides a method for determining appropriate starting models even if the starting background conductivity is incorrect by a few orders of magnitude. The final inversion result using the new 169 Ωm background is shown in Fig. 17. It is a significant improvement over the preliminary inversion in Fig. 15.

With significant topography, even a uniform conductivity model will generate charge build up and anomalous currents. For these geometries it is possible to find the conductivity that best fits the given data. This method is illustrated using a synthetic model of a mountain with a resistor and conductor buried underneath. This model, shown in Fig. 18, has a true background resistivity of 100 Ωm. Data were computed at 960 locations above the mountain. Uniform background models (50, 75, 100, 150, 200 and 250 Ωm) with the correct topography, were forward modelled to obtain data at the same 960 locations. The data misfits between the background and the true models were computed and are shown in Fig. 19. The background that produces the smallest data misfit matches the true conductivity. This method thus allows background models to be created when topography exists and when little additional information is available.

4.3 Assigning uncertainties

Assigning uncertainties to data is a critical step in any geophysical inversion. Overestimating the noise will result in a loss of information which could have been extracted from the data. Similarly, underestimating the noise may create artefacts in the inverted model that are not present in the data. Assigning uncertainties for any geophysical field data set is difficult because there are many error sources, each of which is difficult, if not impossible to quantify. Survey errors such as instrument repeatability, human error, external noise, and misorientation of receivers are often thought to be the only sources of errors that need to be considered in an inversion. These sources are important, however, there are many additional sources of errors such as discretization, modelling approximations, and matrix solution errors. Ultimately, it is difficult to quantify the individual error sources, let alone their sum. Nevertheless it is essential that there is a robust and repeatable method to assign uncertainties to the data.

Unlike some electromagnetic surveys where the dynamic range of the data can vary by several orders of magnitude, ZTEM data generally have small dynamic ranges. Because of this, the standard deviations are assigned as a constant value for each data component. Nevertheless, for field inversions these levels are not known and hence we have used an iterative approach to estimate them. For individual frequencies, each datum is assigned an uncertainty which is a fraction of the dynamic range of the data. Each frequency is inverted separately and then the assigned uncertainties are scaled such that the achieved normalized misfit is unity. This balances the relative importance of each frequency when the simultaneous inversion is carried out. This iterative approach in which the errors on individual frequencies are examined first, before tackling the full inversion problem, ensures that assigning incorrect uncertainties on a few data points, or data associated with a certain frequency, does not ruin the entire inversion.

For the Bingham Canyon inversion, the quality of the data in each component of each frequency was examined. Some regions of the data were removed because they were suspect or because the data were acquired in a region of high power line noise. The dynamic range of each data component (real and imaginary components separately) was determined by sorting the absolute values of the data. The range was assigned to be the difference between the 10th percentile and 90th percentile data. For each frequency and data component, the errors were initially assigned as 12.5 per cent of the range. Inverting each frequency independently ensured the correct data weighting between each frequency. Fig. 20 shows the misfit curve for two frequency components inverted with the initial error estimates. It is clear that the two frequencies need to be scaled by different amounts.

4.4 Bingham Canyon inversion results

Both the real and imaginary components of five frequencies were inverted for the Bingham Canyon ZTEM survey. The inversion was completed without prior knowledge of the geology so no additional

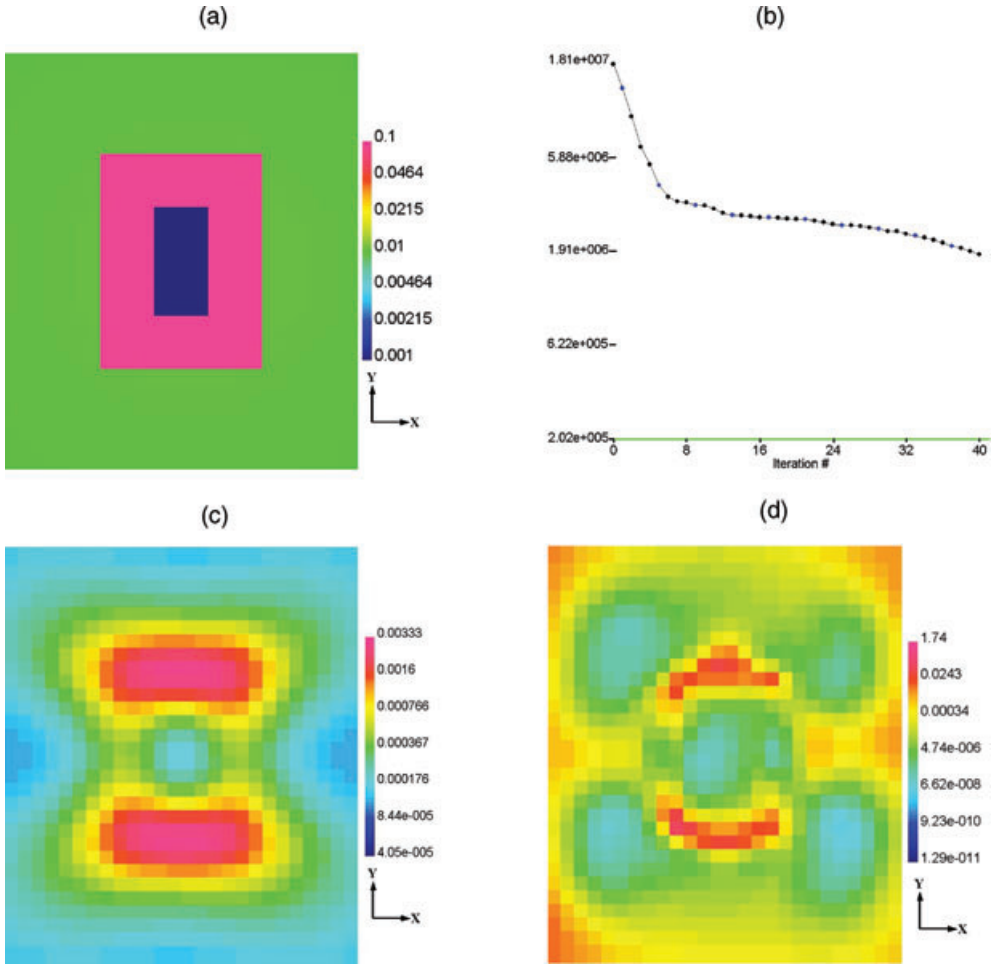

Figure 15. (a) Conductivity (S m^{-1}) of the synthetic true model at a depth of 800 m. (b) Misfit curve. (c) Inverted model at 800 m, using a 10 000 Ωm starting model, taken at the sharp change of slope on the misfit curve. (d) Final inversion model starting with a 10 000 Ωm initial model. The recovered model structure and conductivity values are not reasonable. Here $\alpha_s = 0$, $\alpha_x = \alpha_y = \alpha_z = 1$.

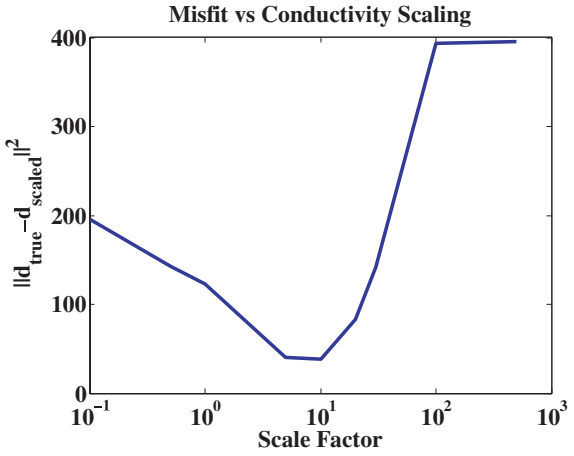

Figure 16. Data misfit for various conductivity scaling factors.

information was incorporated into the inversion. We did however impose respective upper and lower bounds of 2 S m^{-1}–3.33 × 10^{-5} S m^{-1} on the allowed model conductivity for the inversion. The initial and reference models had a constant resistivity of 500 Ωm, and the model smallness parameter, α_s, was set to 10^{-12}. The inversion was run on 5 Intel Xeon 2.33 Ghz dual quad core processors. It took 76 hr to decrease the misfit to 1.59 × 10^6 (target misfit 1.52 × 10^6). After the inversion was completed, a basic geological model for the survey area was obtained. Some surface features in our conductivity model seem to correspond with the local geology. In particular, a well known conducting shale region in the southeast and another conductor to the west have expressions in the inverted model (Fig. 21). Of more economic potential is a feature shown in Fig. 21(b) which coincides with a porphyry outcrop.

5 DISCUSSION AND CONCLUSIONS

The ZTEM technique is a promising method to explore for large scale targets at depth because of easy data acquisition and deep penetration of natural source fields. The data are transfer functions that relate the vertical magnetic field at the observation point to the horizontal fields at a ground based reference station. The reference station is an important component of the system and is needed to compensate for the unknown source field amplitude and polarization. The reference station would ideally be located outside the survey block in a flat region with a 1-D conductivity structure. In practice this is often not possible. However, because the horizontal fields generally have small variations over the survey area and the location of the reference station is modelled in the data, the inversion of ZTEM data is fairly robust with respect to the placement of

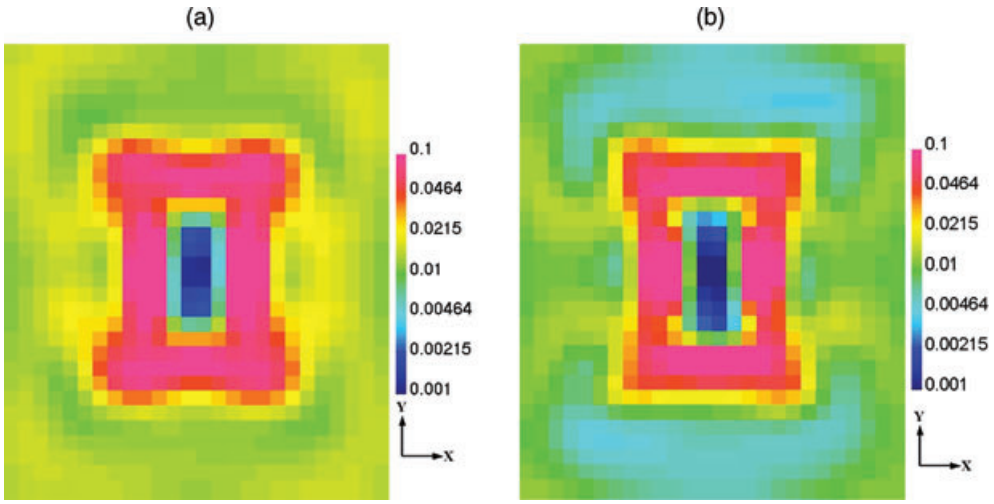

Figure 17. (a) Inverted model (S m^{-1}) at a depth of 800 m starting with the correct initial background conductivity. (b) Inverted model at a depth of 800 m using the scaling method to determine the initial conductivity.

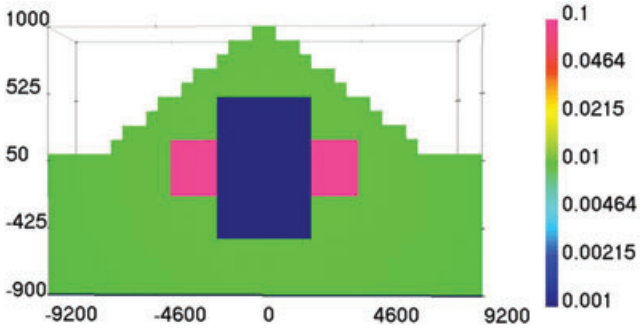

Figure 18. Synthetic test example (S m^{-1}) to show that the method of fitting a best fitting half-space to the data can be used if the model has sufficient topography. The synthetic model has a resistor and conductor buried below a 100 Ωm mountain.

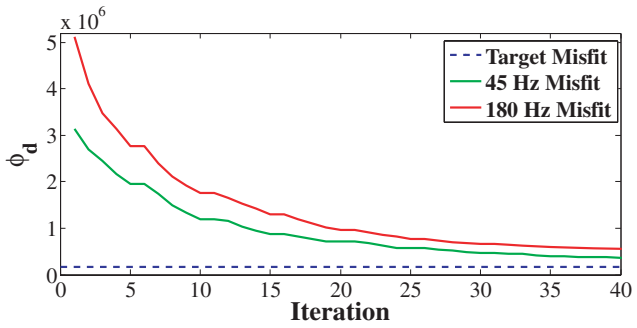

Figure 20. Misfit curve for initial error estimates at 45 and 180 Hz. Even though the same initial error estimates were applied to both frequencies, the assigned errors on the two frequencies must be scaled by different amounts so that they have equal influence in the final inversion. Here $\alpha_s = 10^{-12}$, $\alpha_x = \alpha_y = \alpha_z = 1$.

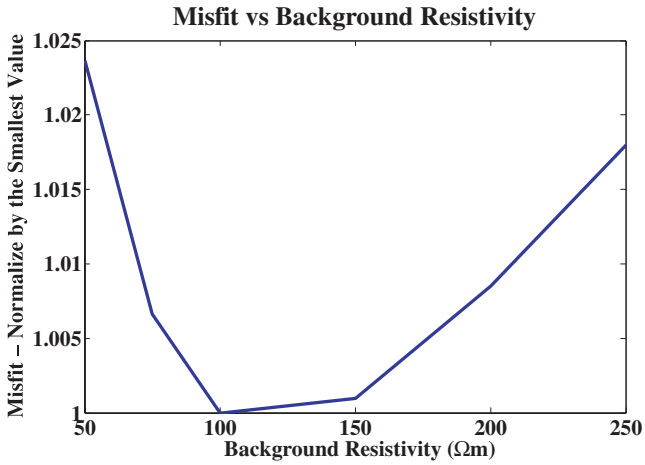

Figure 19. Misfit between the true data and the data produced from different conductivity background models. It is apparent that the 100 Ωm background model which matches the true model background conductivity produces the smallest data misfit.

the reference station. Also, we have shown here that mislocation of reference station may not be critical to a first pass interpretation.

Despite the above comments, there are possible developments with respect to the reference station that may improve ZTEM inversion results. One option would be to use multiple reference locations. A remote reference station (Goubau *et al.* 1978; Gamble *et al.* 1979a,b; Clarke *et al.* 1983) can be used to remove noise from measured magnetotelluric signals and this could be applied to further remove unwanted noise from ZTEM signals. Also, multiple reference stations could be used to obtain information about the horizontal fields in both the background region and the survey area. A natural extension of this idea would be to measure both the vertical and horizontal fields from the helicopter. In this configuration, the data would be the ratio of the vertical field and horizontal field measured at the same location. In addition, it may be possible to derive new useful data from horizontal transfer functions that relate the horizontal field recorded at the helicopter to the horizontal field at a reference station.

In summary, we have developed a 3-D inversion algorithm for ZTEM data using a Gauss–Newton approach. The inversion algorithm shows promising results on a synthetic test problem and illustrates the enhanced depth of penetration that can be obtained by using natural source fields. Because 3-D inversion of

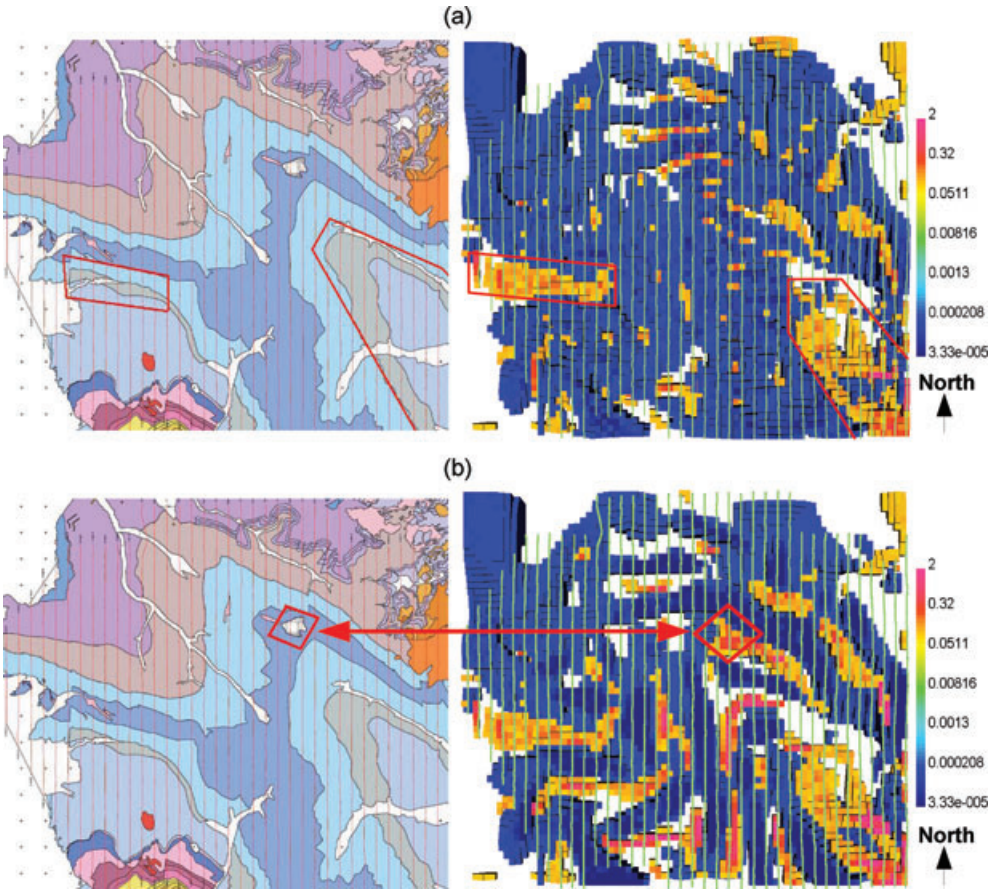

Figure 21. (a) Comparison of the known surface geology (left-hand panel) and inverted model, at the surface, (right-hand panel). There is agreement between the two large known conducting features, outlined in red. The inverted model has cut-offs to show conductors (>0.1 S m^{-1}), and resistors (<0.00025 S m^{-1}). (b) Comparison of a small porphyry outcropping from the geological model and the inverted model viewed at 1600 m. The inverted model has cut-offs to show conductors (>0.1 S m^{-1}), and resistors (<0.00025 S m^{-1}). Note that the inversion places a large conductor directly below the porphyry outcropping.

electromagnetic field data is a complex task, we present the essential inversion elements as a workflow process. Using this approach, field data were inverted from the Bingham Canyon region in Utah. The final inverted model not only fit the data but also showed correspondences with some known geological features from the area.

ACKNOWLEDGMENTS

The authors would like to acknowledge Exploration Syndicate Inc. for providing the data and a geological map of the Bingham Canyon region.

REFERENCES

Clarke, J., Gamble, T., Goubau, W.M., Koch, R. & Miracky, R., 1983. Remote-reference magnetotellurics: equipment and procedures, *Geophys. Prospect.,* **31**(1), 149–170.

Farquharson, C.G., Oldenburg, D.W., Haber, E. & Shekhtman, R., 2002. An algorithm for the three-dimensional inversion of magnetotelluric data, in *Proceedings of the 72nd Annual International Meeting,* SEG, Expanded Abstracts, pp. 649–652.

Gamble, T.D., Goubau, W.M. & Clarke, J., 1979a. Magnetotellurics with a remote magnetic reference, *Geophysics,* **44**(1), 53–68.

Gamble, T.D., Goubau, W.M. & Clarke, J., 1979b. Error analysis for remote reference magnetotellurics, *Geophysics,* **44**(5), 959–968.

Goubau, W.M., Gamble, T. & Clarke, J., 1978. Magnetotelluric data analysis: removal of bias, *Geophysics,* **43,** 1157–1166.

Haber, E., Ascher, U.M., Aruliah, D.A. & Oldenburg, D.W., 2000. Fast simulation of 3D electromagnetic problems using potentials, *J. Comput. Phys.,* **163**(1), 150–171.

Karous, M. & Hjelt, S.E., 1983. Linear filtering of vlp dip-angle measurements, *Geophys. Prospect.,* **31**(5), 782–794.

Labson, V.F., Becker, A., Morrison, H.F. & Conti, U., 1985. Geophysical exploration with audiofrequency natural magnetic fields, *Geophysics,* **50**(4), 656–664.

Lo, B. & Zang, M., 2008. Numerical modeling of z-tem (airborne AFMAG) responses to guide exploration strategies, *SEG Technical Program Expanded Abstracts,* **27**(1), 1098–1102.

Mackie, R.L. & Madden, T.R., 1993. Three-dimensional magnetotelluric inversion using conjugate gradients, *Geophys. J. Int.,* **115,** 215–229.

Newman, G.A. & Alumbaugh, D.L., 2000. Three-dimensional magnetotelluric inversion using non-linear conjugate gradients, *Geophys. J. Int.,* **140,** 410–424.

Saad, Y., 2003. *Iterative Methods for Sparse Linear Systems,* Society for Industrial and Applied Mathematics, Philadelphia, PA, USA.

Sasaki, Y., 2004. Three-dimensional inversion of static-shifted magnetotelluric data, *Earth Planets Space,* **56**(2), 239–248.

Siripunvaraporn, W., Egbert, G., Lenbury, Y. & Uyeshima, M., 2005. Three-dimensional magnetotelluric inversion: data-space method, *Phys. Earth planet. Inter.,* **150**(1–3), 3–14, Electromagnetic Induction in the Earth.

Sundararajan, N., Ramesh Babu, V., Shiva Prasad, N. & Srinivas, Y., 2006. Vlfpros—a matlab code for processing of vlf-em data, *Comput. Geosci.,* **32,** 1806–1813.

Ward, S.H., 1959. Afmag—airborne and ground, *Geophysics,* **24**(4), 761–787.

Ward, S.H., O'Donnell, J., Rivera, R., Ware, G.H. & Fraser, D.C., 1966. Afmag - applications and limitations, *Geophysics,* **31**(3), 576–605.

Zhdanov, M.S., Fang, S. & Hursan, G., 2000. Electromagnetic inversion using quasi-linear approximation, *Geophysics,* **65**(5), 1501–1513.